# Multiscale Tortuous Diffusion in Anion and Cation Exchange Membranes

*Lam M. Thieu,*[a] *Liang Zhu,*[b] *Andrew G. Korovich,*[a]

*Michael A. Hickner,*[b] *and Louis A. Madsen,**[a]

[a]Department of Chemistry and Macromolecules Innovation Institute, Virginia Tech, Blacksburg, VA, 24060

[b]Department of Materials Science and Engineering, The Pennsylvania State University, University Park, PA, 16802

*Louis A. Madsen
Virginia Tech University
Blacksburg, VA 24061
lmadsen@vt.edu

**Keywords:** fuel cell, polymer membrane, NMR diffusometry, restricted diffusion, tortuosity

## Abstract

Fundamental understanding of water transport and morphology is critical for improving ionic conductivity in polymer membranes. In a series of random copolymer anion exchange and cation exchange membranes, we systematically investigate the influence of counterion type, sidechain type, and degree of ionic functionalization on water transport using NMR diffusometry. Time-dependent water diffusion measurements reveal micron-scale heterogeneity of the hydrophilic network in these random copolymers. We propose a model in which the hydrophilic domain network in these membranes has micron-scale distributions of local nm-scale dead ends, leading to changes in tortuosity as a function of water content and membrane composition. We furthermore parse tortuosity into two length-scale regimes, one regime from nanometer (local) to bulk and another from micrometer to bulk, offering enhanced discrimination of the multi-scale morphological structures that influence bulk transport. This study thus provides new insights into ionic polymer membrane morphology and diffusion behavior, with the ultimate goal of controlling polymeric materials for enhanced fuel cells and other separations applications.

## Introduction

Deploying clean energy in place of fossil fuels to reduce carbon dioxide emissions represents a grand challenge of the 21st century. Among emerging technologies, fuel cells show tremendous potential as new energy conversion devices because fuel cells can be zero-emission devices and are not limited by the Carnot cycle.[1] Fuel cells can be classified as operating at low (< 100°C), medium (100 - 200°C), or high (500-1000°C) temperature.[2] Low-temperature fuel cells offer an attractive alternative for producing power that is safe and environmentally friendly for vehicles.[3] The most popular commercial low-temperature fuel cell technology currently available relies on proton exchange membranes or PEMs, such as Nafion®.[4] Due to the acidic environment inside a PEM, these fuel cells usually require precious metals such as platinum (Pt) as anode and cathode catalysts, which is presently the primary determinant of fuel cell cost. While initial results on development of non-Pt catalysts appear promising,[5-6] more studies are needed to reduce the overall price of PEM-based fuel cells.[7-8]

Alternatively, anion exchange membranes (AEMs) are currently under investigation to reduce fuel cell cost by facilitating the use of cheaper catalyst metals, such as nickel or silver.[9-10] Thus, AEMs have received increasing attention from the scientific community.[11-12] Although more than 100 different AEM materials have been reported, examples that can meet all the requirements needed for durable and practical fuel cells are not yet established.[13-16]

Water transport as a function of water uptake is a crucial topic for both AEM and PEM fuel cells.[17] While researchers have extensively studied relationships between water uptake, water diffusion, and conductivity in PEMs,[18-21] systematic research on this topic is limited for AEMs. In 2014, Kreuer et al. reported anion and water transport in poly(arylene ether) membranes with benzyl-tethered quaternary ammonium (QA) cations.[22] They found that even with relatively high

hydration (number of waters per ionic group, $\lambda \sim 10$), the diffusion of water in AEMs under $CO_2$-free conditions is approximately a factor of 2 lower than in cation exchange membranes (CEMs). Furthermore, at lower water uptake ($\lambda < 10$), the extracted diffusion coefficient of hydroxide in AEMs declined more rapidly than the diffusion coefficient of hydronium in PEMs, which they attributed to the less well-defined nanoscale morphology in aromatic AEMs and reduced hydroxide-ammonium pair dissociation in the AEMs. Zhao et al. studied the relationship between water uptake and the diffusion coefficient of water ($D_{H2O}$) in commercial A201 AEM samples (Tokuyama, Japan).[21] The measured $D_{H2O}$ in A201 membrane ($\lambda \sim 15$) showed the same order of magnitude ($10^{-10}$ $m^2/s$) as that of similarly hydrated Nafion membranes ($\lambda \sim 15$). Hibbs et al. also investigated transport property differences between AEMs and PEMs.[23] While $D_{H2O}$ in AEMs (quaternary ammonium-functionalized polysulfone) was greater than in PEMs (sulfonated polyphenylenes), the ionic conductivity and pressure-driven water permeability of AEMs were lower than in PEMs. Herring et al. studied restricted diffusion (dependence of the diffusion coefficient of the mobile species on diffusion time) of water in AEMs.[24] They explained that when the diffusion encoding time, $\Delta$, (and thus the distance or *diffusion length* $l_D$ traveled by the water molecules) increased, $D_{H2O}$ decreased and reached a constant value when $\Delta \geq 50$ ms. Our group has studied the coupling of morphological heterogeneity and water diffusion in block copolymer PEMs[21] as well as in PEM polyelectrolyte-PVDF blend membranes.[19] In the latter study,[19] we observed strong restricted diffusion when the blend components were not optimally compatibilized, and we quantified tortuosity of diffusion for a range of polymer compositions and water contents. As ionic polymer membranes attract ever-increasing attention, new conceptual and methodological studies in this area are needed to better understand the ion and water transport properties (e.g., diffusion and tortuosity) of AEMs, and to develop robust models for the

hydrophilic network in AEMs that facilitates ion transport. Furthermore, determining the influence of chemical modifications such as alkyl sidechains and degree of ionic functionalization on morphology in AEMs, as well as correlating morphology with transport, will enable more informed design of new AEM systems.

In pursuit of these goals, here we investigate the diffusion of water using pulsed-field-gradient (PFG) NMR diffusometry in a systematic set of AEMs and PEMs as a function of varying diffusion time, Δ, and membrane composition. This study uncovers new information regarding the organization of hydrophilic pathways for transport inside these ionic polymer matrices. The AEMs consist of a series of *cationic* poly (2,6-dimethyl-1,4-phenylene oxide) (PPO) benzylquaternary ammonium AEMs with varying alkyl chain lengths.[25] We compare these random copolymer AEMs to random copolymer *anionic* sulfonated poly(ether sulfone) membranes, as well as to the benchmark membrane Nafion. In this work, we investigate anion-containing membranes with both $H^+$ and $K^+$ counterions (to parallel AEMs with $OH^-$ and $Br^-$ counterions), and so from this point forward we will term these cation exchange membanes or CEMs.

Remarkably, we observe that $D_{H2O}$ in these *random copolymer* AEMs and CEMs decreases substantially with increasing Δ, revealing the presence of structural heterogeneities that restrict diffusion on the ~ 1 μm diffusion length ($l_D$) scale probed by the NMR diffusometry experiment. We define and extract two types of tortuosity values from these measurements ("micron-to-bulk tortuosity," $\mathfrak{I}_{\mu-B}$ and "local-to-bulk tortuosity," $\mathfrak{I}_{L-B}$) that we use to understand transport behaviors that depend on membrane morphological structures ranging from nm to μm scales. Finally, for each membrane chemical composition we measure $D_{H2O}$ as a function of water content (volume fraction, $\phi$) as well as diffusion time, Δ. We explore commonalities between diffusion behaviors in AEMs and CEMs of similar chemical structures and counterion type.

We combine all of these measurements to investigate trends in transport spanning a range of polymer membrane compositions under different counterion and hydration conditions, as well as over different time (and length) scales. We draw from these trends to develop models for hydrophilic pathway connectivity and tortuosity behaviors as a function of membrane chemical composition and hydration level. Understanding such chemical structure-morphology-transport behaviors in polymer membranes using NMR diffusometry thus enhances our ability to target enhanced performance of AEMs for next generation fuel cells and other molecular and ionic separations applications.

## Materials and Methods

### *Polymer membranes*

There are four series of samples described in this work: AEMs, synthesized in the bromide ($Br^-$) form and then ion exchanged to hydroxide form ($OH^-$), and CEMs, purchased from YANJIN Technology Co., Ltd. in the potassium ($K^+$) form and then ion exchanged to proton form ($H^+$). The CEMs are random copolymers of sulfonated poly(ether sulfone) with varying degrees of functionalization (DF) (percentage of monomers with ionic functionality) from 20% to 60%.[26] The AEMs are random copolymers of cationic benzyltrimethyl quaternary ammonium poly(2, 6-dimethyl-1,4-phenylene oxide) (PPO), with a fixed DF of 40%.[25,15] The AEMs were cast in the $Br^-$ form, then converted from $Br^-$ to $OH^-$ by immersing in 1 M NaOH under $N_2$ atmosphere for 48 hours with thorough rinsing. Similarly, the CEMs were cast in the $K^+$ form, then converted from $K^+$ form to $H^+$ form by immersing samples in 1 M HCl for 48 hours under ambient conditions. The chemical structures and sample information are shown in **Scheme 1** and **Table 1**, respectively.

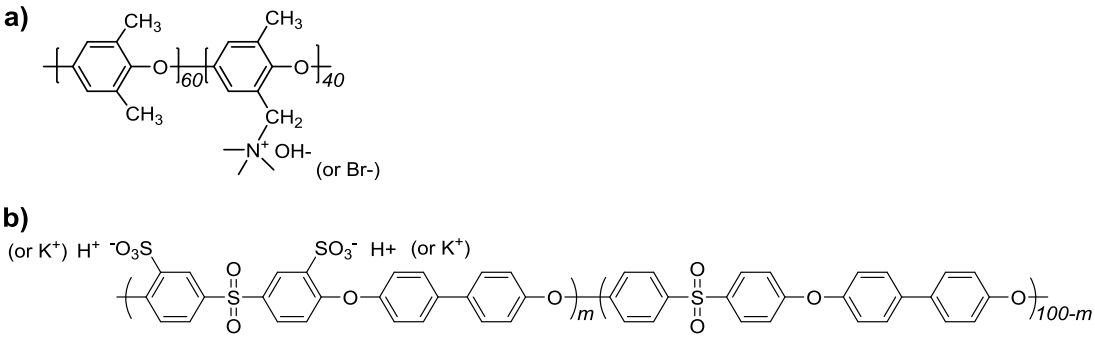


**Scheme 1.** Chemical structures of a) cationic quaternary ammonium poly(2,6-dimethyl-1,4-phenylene oxide) (PPO) AEM (hydroxide and bromide form) and b) anionic sulfonated poly(ether sulfone) CEM (proton and potassium form).

**Table 1.** Summary of sample information for anion exchange and cation exchange membranes.

| Type | Sample | Counter-ion | DF (%) | IEC (meq/g) | Wt.% $H_2O$ (Saturated) | Vol. fraction $H_2O$ ($\Phi$) | $\lambda$ |
|---|---|---|---|---|---|---|---|
| AEM | **AEM_BTMAD40 (x = 1) (BTMA)** | $OH^-$ | 40 | 2.67 | 130 | 0.62 | 27 |
| | **AEM_C6D40 (x=6) (C6)** | $OH^-$ | 40 | 2.25 | 66 | 0.43 | 16 |
| | **AEM_C10D40 (x=10) (C10)** | $OH^-$ | 40 | 2.00 | 46 | 0.34 | 13 |
| | **AEM_C16D40 (x=16) (C16)** | $OH^-$ | 40 | 1.71 | 54 | 0.38 | 18 |
| | **AEM_BTMAD40 (x=1) (BTMA)** | $Br^-$ | 40 | 2.28 | 33 | 0.29 | 8.0 |
| | **AEM_C6D40 (x=6) (C6)** | $Br^-$ | 40 | 1.97 | 21 | 0.19 | 5.8 |
| | **AEM_C10D40 (x=10) (C10)** | $Br^-$ | 40 | 1.77 | 19 | 0.18 | 5.9 |
| | **AEM_C16D40 (x=16) (C16)** | $Br^-$ | 40 | 1.54 | 22 | 0.20 | 7.9 |
| CEM | **CEM_D60 (m=60) (D60)** | $H^+$ | 60 | 2.42 | 96 | 0.59 | 22 |
| | **CEM_D50 (m=50) (D50)** | $H^+$ | 50 | 2.08 | 65 | 0.48 | 17 |
| | **CEM_D40 (m=40) (D40)** | $H^+$ | 40 | 1.72 | 42 | 0.36 | 14 |
| | **CEM_D30 (m=30) (D30)** | $H^+$ | 30 | 1.34 | 29 | 0.27 | 12 |
| | **CEM_D20 (m=20) (D20)** | $H^+$ | 20 | 0.93 | 68 | 0.46 | 41 |
| | **CEM_D60 (m=60) (D60)** | $K^+$ | 60 | 2.22 | 55 | 0.46 | 14 |
| | **CEM_D50 (m=50) (D50)** | $K^+$ | 50 | 1.93 | 30 | 0.30 | 8.6 |
| | **CEM_D40 (m=40) (D40)** | $K^+$ | 40 | 1.62 | 27 | 0.27 | 9.2 |
| | **CEM_D30 (m=30) (D30)** | $K^+$ | 30 | 1.27 | 19 | 0.19 | 8.4 |
| | **CEM_D20 (m=20) (D20)** | $K^+$ | 20 | 0.89 | 41 | 0.33 | 26 |

The IEC was calculated from the titrated equivalent weight of the polymer and compared with the IEC from the literature.[25] Each sample name is expressed as follows. The type of

membrane, AEM or CEM, is followed by the number of carbons in the alkyl chain (C6, C10, C16), then the degree of functionalization DF, then the counterion type. For example, AEM_C16D40_OH (C16_OH in short) refers to an anion exchange membrane with 40% functionalized monomers (DF), with an attached 16-carbon alkyl side chain, and in the hydroxide counterion form. CEM_D20_K (D20_K in short) refers to a cation exchange membrane with DF = 20%, no alkyl sidechain, and in the potassium counterion form. In total, there are 8 AEMs: BTMA, C6, C10, and C16 with each in $OH^-$ and $Br^-$ form, and 10 CEMs: D20, D30, D40, D50, and D60 with each in $H^+$ and $K^+$ form.

***NMR sample preparation***

Membranes were cut into 4 mm × 4 mm sample pieces, stacked together (6-14 layers to enhance the NMR signal) and wrapped with PTFE tape. Each sample stack was soaked in deionized water for at least 48 hours to obtain saturated water uptake, then quickly blotted with a Kimwipe to remove surface water and wrapped in LDPE plastic food wrap. Finally, each sample was sealed inside a custom PTFE cell, designed for an 8 mm coil, with low dead (gas) volume[19-21] to eliminate water content changes during NMR analysis. An equilibration time of 30 min after sealing was used for membrane samples before NMR measurement. To control the water content, the sample was removed from the cell and left on the balance for water to evaporate until it achieved the desired mass ($mass_{wet}$). After finishing the NMR experiments, each sample was dried in a vacuum oven at 60 °C overnight to obtain the dry mass ($mass_{dry}$). Water content was determined using

$$wt.\%\ H_2O = \frac{mass_{wet} - mass_{dry}}{mass_{dry}} \times 100\ . \quad (1)$$

Water content (*wt. %*) can be convert to water volume fraction ($\phi$) by

$$\phi = \frac{wt.\%\ H_2O/100}{wt.\%\ H_2O/100 + \frac{\rho_{water}}{\rho_{polymer}}}, \quad (2)$$

in which, $\rho_{water}$ and $\rho_{polymer}$ are the density of water and polymer respectively (g/mL) (See table S1-Supporting Information for the density of polymers. We assume $\rho_{CEM\_K} \approx \rho_{CEM\_H}$ and $\rho_{AEM\_Br} \approx \rho_{AEM\_OH}$).

For membrane samples, water content was converted to lambda ($\lambda$) (number of $H_2O$ per polymer-fixed anionic or cation site) by

$$\lambda = \frac{wt.\%\ H_2O \times 10}{IEC \times M_{water}}, \quad (3)$$

in which $wt.\%\ H_2O$ is the water content, $IEC$ represents ion-exchange capacity (meq/g), and $M_{water}$ is the molecular weight of water in g/mol.

For acid and base solution samples (see **Figure 4** below), tetramethylammonium hydroxide ($(CH_3)_4NOH$, as 25 wt.% solution), p-toluenesulfonic acid ($CH_3C_6H_4SO_3H$, as monohydrate, 99%), and trifluoromethanesulfonic acid ($CF_3SO_3H$, 99%) were obtained from Sigma-Aldrich and used without modification except for dilution with deionized water. $\lambda$ is the molar ratio of $H_2O$ to ion pair in the liquid solution, determined gravimetrically when mixing the solutions by

$$\lambda = \frac{1000}{C_M M_{water}} \quad (4)$$

where $C_M$ is the molal concentration of ions in solution (mol/kg).

***Pulsed-field-gradient (PFG) NMR diffusometry***

$^1H_2O$ self-diffusion measurements were performed at 22 °C using the pulsed-gradient stimulated echo (PGSTE) NMR pulse sequence on a Bruker Avance III 9.4T wide-bore spectrometer corresponding to a $^1H$ frequency of 400.13 MHz. A magnetic resonance imaging probe ("Bruker Micro5") equipped with triple-axis gradients and an 8 mm $^1H$ radio frequency coil

was used. The NMR signal attenuation due to diffusion is described by the Stejskal-Tanner equation[27]

$$I = I_0 e^{-Dy^2 g^2 \delta^2 \left(\Delta - \delta/3\right)} = I_0 e^{-Db} , \quad (5)$$

where $I$ is the spin-echo signal intensity at a given gradient strength $g$ (maximum values used in the range 20 – 300 G/cm), $I_0$ is the signal intensity at zero gradient, and $\gamma$ is the gyromagnetic ratio of $^1$H nucleus (26752 rad s$^{-1}$G$^{-1}$). $\delta$ (= 2 ms) is the effective rectangular length of the gradient pulse (actual half sinusoid gradient pulse length was $\delta$ = 3.14 ms), $\Delta$ (= 8 ms to 1 s) is the diffusion encoding time or duration between the two gradient pulses, and $b$ is the Stejskal-Tanner (signal attenuation) factor that encompasses all known NMR-specific experimental parameters. The observed spin relaxation times $T_1$ and $T_2$ varied from 250 ms to 1500 ms and 8 ms to 150 ms, respectively. The PGSTE sequence was used with 90° pulse lengths = 6 $\mu$s in duration and each diffusion experiment used eight gradient steps and 16 scans per step. $D$ is the self-diffusion coefficient of the mobile species extracted by fitting the signal attenuation ($I/I_0$) curve as a function of $g$ with **Equation 4**.

## Results and Discussion

### *Measuring diffusion coefficient of water in AEMs and CEMs*

**Figure 1a** shows the 1D pulse-acquire $^1$H-NMR spectrum of water in AEM_BTMA_OH at a volume fraction $\phi$ = 0.46 $H_2O$. We observe a broad peak and a narrow single peak corresponding to polymer and water NMR signals, respectively. The water peak in AEM_BTMA_OH includes both $OH^-$ and $H_2O$ species, but the exchange process between these species occurs too rapidly for NMR to distinguish their separate signals. The obtained diffusion coefficient of water, $D_{H2O}$, is thus an average of these species, which holds true for acidic species

and water in CEMs. In the PFG NMR diffusometry experiment, the broad polymer peak was suppressed due to relaxation time weighting from the diffusometry experiment, and we obtained only the narrow peak as illustrated in **Figure 1b**. We applied NMR diffusometry to determine $D_{H2O}$ through an 8-step attenuation process with signal intensity obtained by integrating the narrow water peak (see **Figure S1**). **Figure 1c** displays representative signal attenuation curves for measurement of $D_{H2O}$ in AEM_BTMA_OH ($\phi$ = 0.46 $H_2O$), AEM_C6_OH ($\phi$ = 0.26), and CEM_D50_K ($\phi$ = 0.42) with fitted $D_{H2O}$ values shown on the plot.

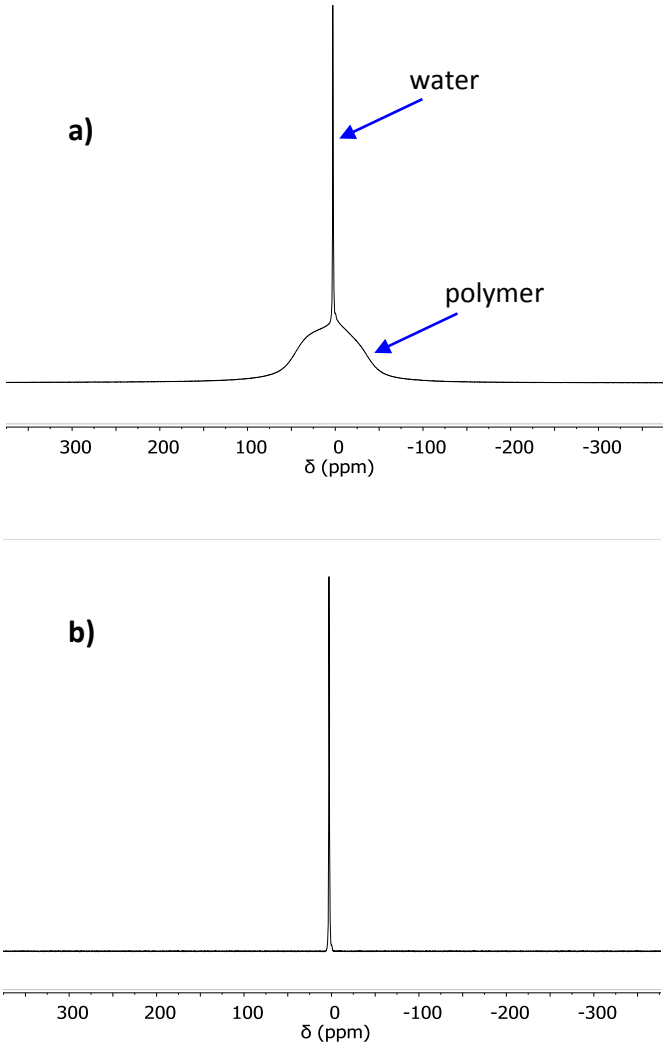

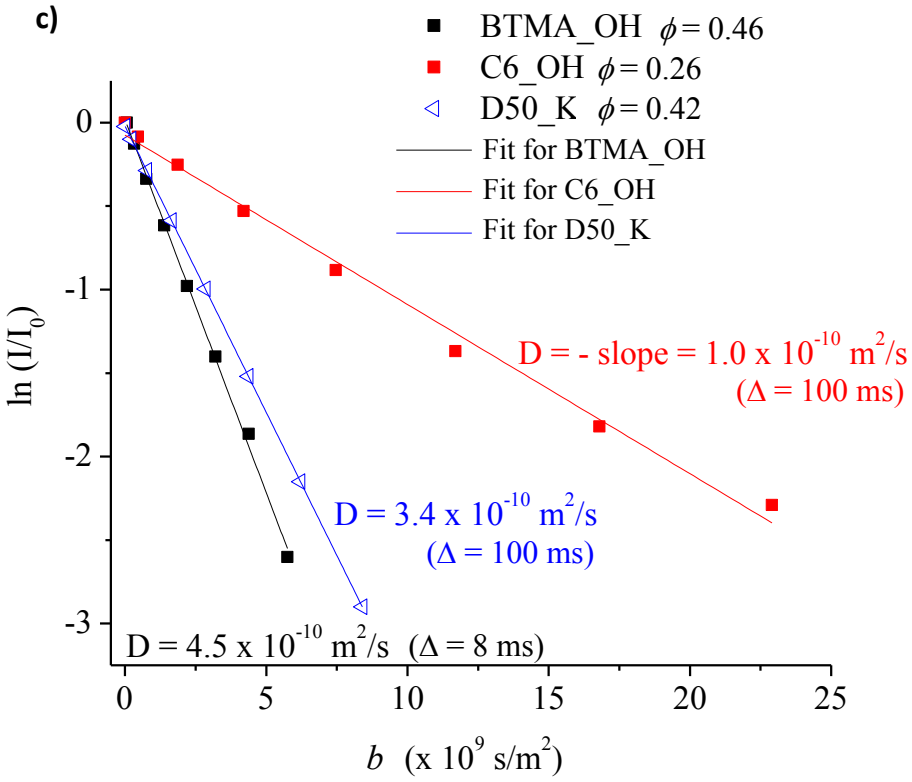


**Figure 1.** a) 1D pulse-acquire $^1$H-NMR of AEM_BTMA_OH ($\phi$ = 0.46) at 22°C. The broad peak and the narrow peak correspond to polymer and water, respectively. b) The first slice (1D spectrum) of the 2D NMR diffusometry experiment for AEM_BTMA_OH ($\phi$ = 0.46). The broad peak is removed by the PFG NMR pulse sequence, and only the narrow (water) peak remains. c) Normalized NMR signal intensity ln ($I/I_0$) vs. Stejskal-Tanner (signal attenuation) factor $b$ for AEM_BTMA_OH ($\phi$ = 0.46), AEM_C6_OH ($\phi$ = 0.26) and CEM_D50_K ($\phi$ = 0.42). The negative slope of the fit line is the diffusion coefficient. Diffusion times Δ are shown in parentheses for each experiment. Estimated errors in diffusion coefficients are ±5%.

In the next section, we explore multi-scale heterogeneity effects on water diffusion in AEMs and CEMs through the use of "restricted diffusion" measurements ($D_{H2O}$ vs. diffusion

encoding time Δ) combined with concepts of tortuosity. Furthermore, we investigate the trends in water diffusion as a function of counterion type, membrane composition, and water uptake.

***Diffusion of water as a function of observation time: Restricted diffusion***

In the NMR diffusometry experiment, we have an adjustable *diffusion time*, Δ, which can generally range from a few ms to ~ 1 s. This variable is therefore a controllable time period over which we observe self-diffusion, and we can easily convert this to *diffusion length* $l_D$ by

$$l_D = < r^2 >^{1/2} = \sqrt{2D\Delta}\,, \tag{6}$$

where $<r^2>^{1/2}$ is the root-mean-square displacement that molecules undergo during the NMR diffusometry experiment.[28-29] $l_D$ ranges typically from ~ 100 nm up to ~ 10 μm depending on the values of $D$ and Δ, thus providing access to correlations between morphological heterogeneity on these length scales and the observed diffusion coefficient $D$. The systematic measurement of $D$ as a function of Δ is known as a "restricted diffusion" study, and here we explore this length-scale-dependent variation of diffusion coefficient in AEMs and CEMs.

**Figure 2** displays the relationship between $D_{H2O}$ and the diffusion time Δ of water inside AEM_OH and CEM_H at a controlled water volume fraction $\phi \sim 0.2$ for all membranes (part a), and under saturated conditions (part b). Both CEM_H and AEM_OH display a roughly similar trend: As Δ increases, water molecules interact with heterogeneous restrictions (such as domain boundaries or walls) leading to a decrease in $D_{H2O}$, usually to an asymptotic value at long times. Among AEM_OH membranes, BTMA_OH absorbs the most water, resulting in the highest diffusion coefficient $D_{H2O} = 7.4 \times 10^{-10}$ m$^2$/s at Δ = 8 ms and corresponding to a diffusion length $l_D = 2.4$ $\mu$m. $D_{H2O}$ decreases to $4.8 \times 10^{-10}$ m$^2$/s at Δ = 512 ms or $l_D = 15.6$ $\mu$m. AEM_C6_OH, AEM_C10_OH, and AEM_C16_OH exhibit the same phenomenon. Compared to AEMs, $D_{H2O}$

for CEMs has a weaker dependence on Δ demonstrating that CEM_H has a less restricted micron-scale hydrophilic transport network (morphology) than AEM_OH. We note that $D_{H2O}$ in extruded Nafion 117 is independent of Δ, with Δ ranging from 4 ms to 1000 ms.[30-31]

At saturated water uptake for the samples, $D_{H2O}$ in AEM_OH and CEM_H samples vary widely because diffusion depends strongly on how much water the membrane can absorb. Nevertheless, if we fix the water content for all membranes to a common value (*ca.* $\phi = 0.2$), $D_{H2O}$ data for all AEM_OHs overlay, where for all membranes $D_{H2O}$ decreased from approximately $7 \times 10^{-11}$ m$^2$/s at $\Delta = 8$ (or $l_D = 0.8$ $\mu$m) to $2 \times 10^{-11}$ m$^2$/s at diffusion time of $\Delta = 512$ (or $l_D = 2.7$ $\mu$m). On the other hand, $D_{H2O}$ curves for different CEM_H membranes do not collapse as neatly onto one trend line. In Figure 2a, we note a plateau in the diffusion coefficients for the CEM_H membranes at diffusion times shorter than 100 ms (or $l_D$ = 4.8 $\mu$m), indicating that these measurements are exploring length scales below the length scale where heterogeneities start to influence diffusion in the hydrophilic network. This plateau is not observed in the AEM_OH measurements, indicating heterogeneities in these membranes exist both below and on the length scale probed by our shortest diffusion length, $l_D = 0.8$ $\mu$m. Under saturated water uptake conditions (**Figure 2b**), we further observe that the decline in diffusion coefficient for both CEM_H membranes occurs at longer diffusion lengths, indicating an increase in the characteristic length scale of heterogeneities in these samples as compared to AEM_OH samples.

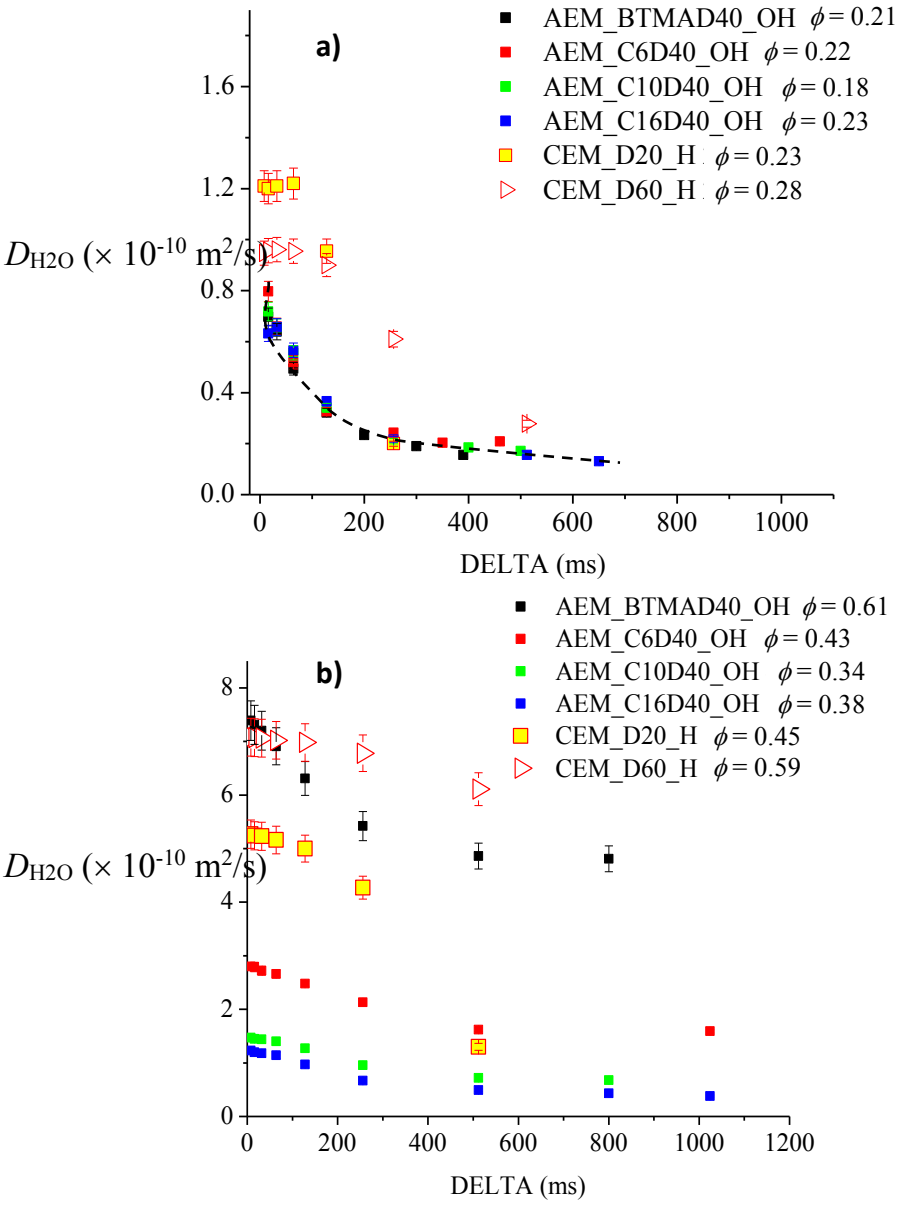


**Figure 2.** Water diffusion $D_{H2O}$ vs. diffusion time Δ for AEM_OH and CEM_H at 22°C at a) comparable water uptake ($\phi \sim 0.2$) and b) saturated water uptake. The black dashed line is a guide to the eye. At comparable water content, AEMs closely follow a trend curve while CEMs do not. At saturation, all membranes show restricted diffusion, although CEMs show decreasing $D_{H2O}$ only at longer Δ values (> 100 ms). Error bars for $D_{H2O}$ are ±5% at short Δ and ±10% for long Δ.

We note here that these are all random copolymer systems with no apparent long-range order. For the AEMs, we conducted small-angle X-ray scattering (SAXS, see **Figure S6**), which showed rather broad peaks with nm-scale features characteristic of ionic clusters in random copolymers. The AEMs exhibited differences in feature size related to alkyl sidechain length.[25] We furthermore observed no characteristic or periodic structural differences with scanning electron microscopy (SEM) on the μm length scales that we probed with NMR diffusometry here. Future work will encompass other attempts to resolve μm-scale structure using microscopy with heavy metal contrast additives, such as ultrasmall angle X-ray scattering (USAXS) and/or neutron scattering. In the absence of these other techniques, diffusion-time-dependent NMR diffusometry provides a distinct probe of μm-scale morphological structure, and one that also directly links particular time and length scales to molecular transport. In order to further parse the length scales of organization in these polymer membranes and their effects on transport, in the next section, we explore the idea of *tortuosity averaged over different length scales*.

***Multi-scale tortuosity in membranes***

Consider a water molecule diffusing in a confined pore with radius $R$.[29, 32-34] Assume the pore has reflecting walls, in which the particle cannot move through the wall or boundary. If the mean-square displacement, or square of the diffusion length $l_D^2 = D\Delta$ is less than $R^2$, which is equivalent to the displacement of the molecule being smaller than the radius of the pore, then the molecule does not experience the confined pore. In this regime, the molecule experiences what we define as the local diffusion coefficient ($D_{loc}$), which is independent of Δ and is depicted in **Figure 3a**. If $l_D^2 = D\Delta \sim R^2$, a fraction of the molecules will feel the effects of the pore boundary, leading to a decrease in observed $D$. If $l_D^2 = D\Delta >> R^2$, the obtained diffusion coefficient will directly reflect the tortuosity ($\mathfrak{I}$) of the network.[35] This model has seen wide application in a wide array

of porous media (usually hard materials),[33] and has recently found use in water swollen domains in polymeric systems such as PEMs[19] and solvent-swollen block copolymers.[36] In these cases, boundaries may not be hard walls, but instead can represent μm-scale heterogeneity, such as a grain boundary or complex domain structure. Within each grain, polymer morphology is locally ordered. The grains may be separated by less (or more) conductive boundary layers, which may, e.g., represent groupings of defects, or agglomerations of one type of phase (hydrophilic or hydrophobic).[21, 36-38]

Tortuosity, $\mathfrak{T}$, is an important parameter that describes interconnected porous networks. A lower $\mathfrak{T}$ represents a more fully connected network with more direct paths for diffusion. $\mathfrak{T}$, as averaged over all length scales above the local molecular scale, can be defined in terms of diffusion coefficients as shown in **Equation 6**.[39]

$$\mathfrak{T} = \frac{D_{loc}}{D_{\infty}} \tag{7}$$

In this study, $D_{loc}$ represents the local diffusion coefficient that water molecules would experience within each nm-scale hydrophilic pore, as depicted in **Figure 3a**. While nanoconfinement effects may influence this intra-pore diffusion,[40] here we make the simplfying approximation that $D_{loc}$ is the diffusion coefficient of a bulk liquid solution with a similar ion concentration and ion type to that in a given membrane's interior (see below). $D_{\infty}$ is the diffusion coefficient of the probe molecule at infinite diffusion time $\Delta$ (or length $l_D$), as depicted in **Figure 3b**. $\mathfrak{T}$ necessarily is $\geq 1$, where $\mathfrak{T} = 1$ is the tortuosity of a pure isotropic liquid with no restrictions to motion.

PFG NMR diffusometry has been widely applied to characterize the tortuosity of conventional macroporous materials by measuring $D$ for probe molecules inside pores as a

function of Δ.[29, 33] For example, if we use water as the molecular probe and measure the diffusion coefficient with Δ = 10 ms, the diffusion length $l_D$ = 7 μm ($< r^2 >^{1/2} = \sqrt{2D\Delta}$ = $\sqrt{2 \times 2.3 \times 10^{-9} \times 10^{-2}} = 6.8 \times 10^{-6}$ m), which is about the pore size of a conventional macroporous material such as a rock. For polymer membranes, NMR diffusometry thus can extract observed $D_{H2O}$ over a range of length scales spanning approximately 0.1 to 100 μm (depending on the Δ employed and the observed $D$). This includes $D_\infty$, the bulk diffusion coefficient through the whole membrane.

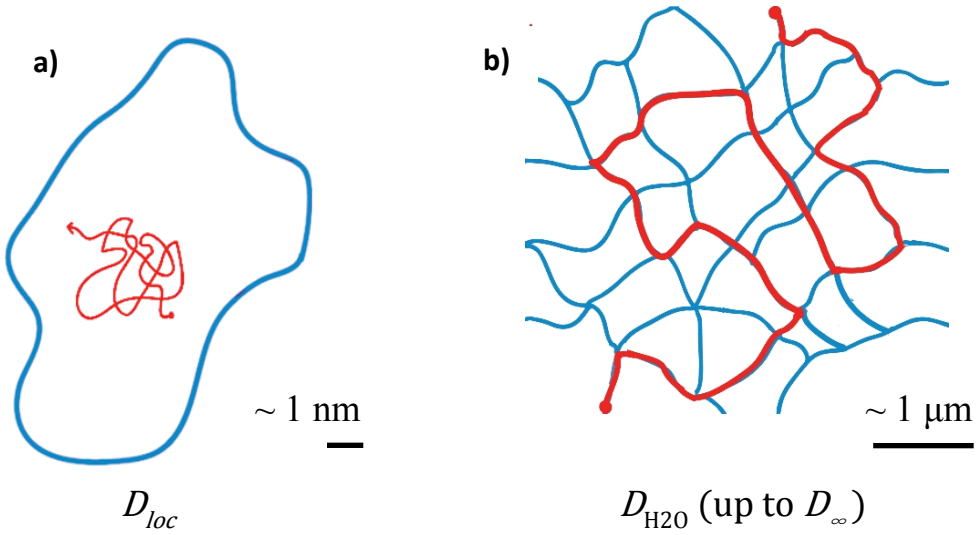


**Figure 3.** Illustration of diffusion concepts relevant to tortuosity of a PEM hydrophilic transport network. a) A water molecule diffuses locally inside a nm-scale hydrophilic cavity. b) Water follows a tortuous path through the interconnected hydrophilic network (of nm-scale cavities) at ms and longer timescales.

We can consider AEMs and CEMs to be water-swollen porous materials, in which the hydrophobic part of the polymer forms a structural matrix and the hydrophilic cavities form a water-filled porous network.[19] Since the hydrophilic cavities in PEMs have diameters on the order

of nanometers, we observe a long-time (ms) and μm-scale average using NMR diffusometry, as given by the timescale of the measurement, Δ. However, we can vary Δ to measure different $D_{H2O}$ values that encompass any μm-scale heterogeneities in the membrane.[19, 41] If we minimize Δ, (with a lower limit of a few ms) we measure what we define as $D_{0,micro}$. $D_{0,micro}$ represents $D_{H2O}$ averaged over the smallest length accessible by NMR diffusometry, usually ≥ 0.1 μm. Thus, we can subdivide the porous network tortuosity into two separate parameters:

$$\mathfrak{I}_{L-B} = \frac{D_{loc}}{D_{\infty}} \tag{8}$$

$$\mathfrak{I}_{\mu-B} = \frac{D_{0,micro}}{D_{\infty}} \tag{9}$$

To summarize, $\mathfrak{I}_{L-B}$ is the "local-to-bulk tortuosity," which averages over structures that range all the way from local molecular scales (nm) to bulk, while $\mathfrak{I}_{\mu-B}$ is the "micron-to-bulk tortuosity," which arises from morphological heterogeneities that range from micrometer scale to bulk.

Specifically in this study, we take $D_{loc}$ to be the diffusion coefficient of water obtained in free liquid solutions as shown in **Figure 4** and **Table S3**, where for AEMs we use tetramethylammonium hydroxide ($(CH_3)_4NOH$) as the local diffusion standard, for the aromatic-based CEMs we use p-toluenesulfonic acid ($CH_3C_6H_4SO_3H$), and for Nafion we use trifluoromethanesulfonic acid ($CF_3SO_3H$).[40] In free solution, the diffusion coefficient of water will be *independent of diffusion length*, and therefore these solution data represent an approximate model of the local (molecular-scale) diffusion coefficient of water in the AEMs and CEMs, as depicted in **Figure 3a**. For each solution used to determine $D_{loc}$ for a given membrane composition and hydration, we adjust the solution lambda to mimic lambda inside the membrane. $D_{\infty}$ is the

diffusion coefficient measured in the membrane at the largest Δ accessible due to the limitations in water $^1$H $T_1$ relaxation time.[19] By employing the above analysis, $\Im_{L-B}$ and $\Im_{\mu-B}$ provide quantitatively separable insights into how molecular transport is affected by morphological structures over widely different length scales in polymer membranes. Further refinements to this model are underway, focusing especially on the aspects of intra-pore nanoconfinement and local molecular environment.[40, 42-43]

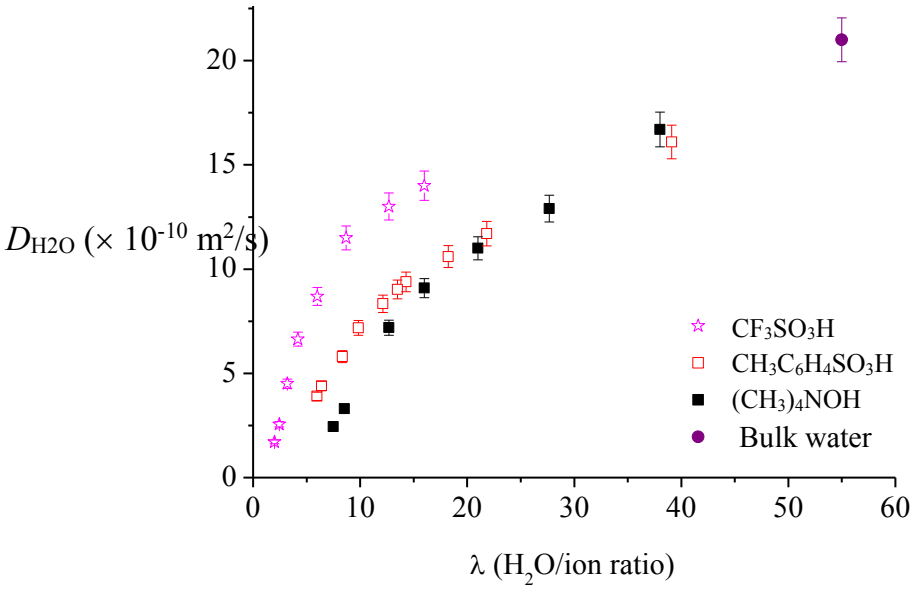


**Figure 4.** $D_{H2O}$ obtained by $^1$H NMR diffusometry as a function of water-ion mole ratio λ for trifluoromethanesulfonic acid ($CF_3SO_3H$),[40] p-toluenesulfonic acid ($CH_3C_6H_4SO_3H$), and tetramethylammonium hydroxide ($(CH_3)_4NOH$) as free liquid solutions. These diffusion coefficients approximate the local diffusion of water ($D_{loc}$) inside AEMs and CEMs. All measurements were performed at 22°C and using Δ = 25 ms. Note that for these isotropic liquid solutions, $D_{H2O}$ is completely independent of Δ.

**Figure 5** shows $\Im_{L-B}$ and $\Im_{\mu-B}$ for both CEMs and AEMs as a function of water content. Additionally, all information concerning tortuosity and measured diffusion coefficients for

membranes and free solutions is summarized in **Tables S2** and **S3**. As shown in **Figure 5a**, $\mathfrak{I}_{L-B}$ strongly depends on water uptake, where the membranes show between a factor of 1.5 and 5 drop in $\mathfrak{I}_{L-B}$ with increasing water content. AEM_BTMA_OH absorbed the most water, resulting in a low $\mathfrak{I}_{L-B}$ at saturated water content, although at $\phi \sim 0.2$ water content, AEMs with the longer alkyl sidechains (C6 and C10) matched the $\mathfrak{I}_{L-B}$ of BTMA. AEM_C16_OH showed substantially higher $\mathfrak{I}_{L-B}$ regardless of water content and we note that conductivity for C16 is also lower than for C10.[25] Although there is a greater extent of phase separation for C16 (see **Figure S6**), we hypothesize that the additional hydrophobic component could cause restrictions to connectivity, potentially due to less connected nm-scale pathway formation arising from the long alkyl sidechain substituent. Among CEMs, D20 showed the highest $\mathfrak{I}_{L-B}$, assumedly related to its low degree of (hydrophilic) functionalization that provides for poor nanophase separation or self-assembly and thus weak hydrophilic cavity connectivity relative to D60. In general, the measured tortuosity of CEMs is higher than in AEMs, indicating that overall the water transport *pathway connectivity* in CEMs is more restrictive than AEMs. Since in general CEMs have faster overall diffusion than AEMs (**Figure 2a**) at equivalent water content, this emphasizes that the *local molecular effects* contributing to faster bulk diffusion[40, 44] in CEMs outweigh the inferior tortuosity (pathway connectivity) effects.

**Figure 5b** displays the relationship between micron-to-bulk tortuosity $\mathfrak{I}_{\mu-B}$ as a function of water content, which is substantially smaller in both CEMs and AEMs as compared to $\mathfrak{I}_{L-B}$. $\mathfrak{I}_{\mu-B}$ represents the degree of "disconnectivity" of water pathways, but only representing ~ 1 μm and larger scales. This parameter indicates that for many of these membranes (especially the CEMs), the *nm-scale to μm-scale heterogeneities* (simply obtained from the difference $\mathfrak{I}_{L-B} - \mathfrak{I}_{\mu-B}$) dominate over the larger scale heterogeneities ($\mathfrak{I}_{\mu-B}$). For most of the AEMs on the other

hand, we see that $\Im_{L-B}$ is much closer to $\Im_{\mu-B}$, indicating that the hydrophilic cavities are well connected below the μm scale. We believe this is the first instance of parsing the influence of subtle multi-scale heterogeneities on bulk transport. For such random copolymer systems, we were surprised to find such strong effects due to μm-scale hetergeneity ($\Im_{\mu-B}$). We propose a basic morphology model below that is consistent with the observations presented in **Figure 5**.

We note that these restricted diffusion observations contain information interpretable as the surface-area-to-volume ratio of the confined geometry, as shown by Mitra et al.[32, 34] We consider this analysis is more complex and currently not subject to concrete interpretation in these random copolymer systems, as compared to the above tortuosity analysis. However, we have placed relevant information extracted from our fits of diffusion coefficients to the Mitra equation in **Figure S5** and **Table S4**.

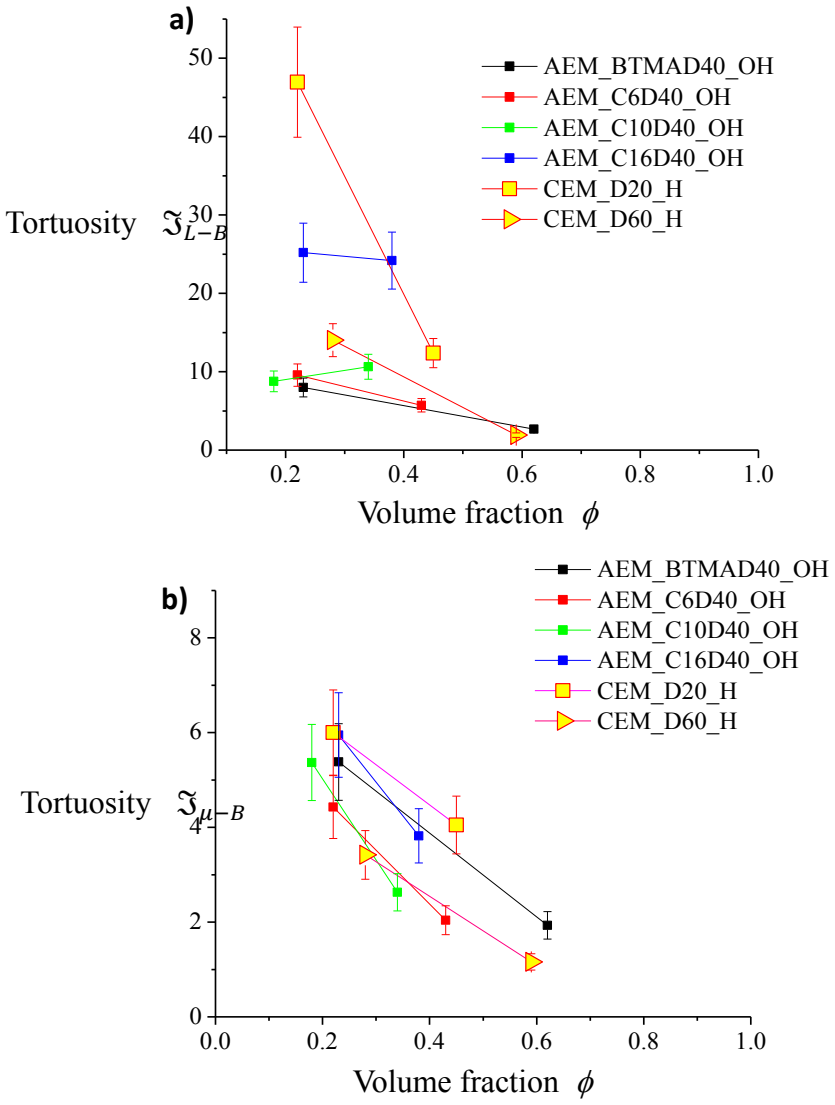


**Figure 5.** Tortuosity of AEMs and CEMs separated into two length scale ranges. a) Tortuosity from local to bulk ($\Im_{L-B}$) as a function of water volume fraction $\phi$. b) Tortuosity from micron to bulk ($\Im_{\mu-B}$). $\Im_{L-B}$ for CEMs is substantially higher than for AEMs (especially at low water content), indicating that the nm-scale connectivity (morphology) is worse than in AEMs. $\Im_{\mu-B}$ values are more similar among all membranes as compared to $\Im_{L-B}$, indicating a general similarly of μm-scale heterogeneities in these membranes. Error bars originate from combining errors for the appropriate ratios of diffusion coefficients involved ($D_{loc}$, $D_{0,micro}$, and $D_{\infty}$).

Based on these measurements of tortuosity parameters, here we present a simple picture for the influence of water-content-dependent cavity (ionic domain) connectivity on water transport (**Figure 6**). **Figure 6a** illustrates the nm-scale hydrophilic cavity network inside a membrane at low, medium and high water content. At low hydration, these ~ 1 nm size hydrophilic cavities (containing clusters of polymer-fixed ions and their associated counterions) are collapsed, resulting in a poorly interconnected hydrophilic network and more restricted (slower) overall bulk transport. At medium hydration, the hydrophilic cavities expand to bridge some "dead ends," resulting in a better interconnected network. At high hydration, the hydrophilic cavities (ionic domains) grow even larger and form a more strongly connected network. **Figures 6b** and **6c** illustrate the consequences of more strongly interconnected networks, where dead ends may cluster together so as to create micrometer-scale heterogeneity that is reflected in the NMR restricted diffusion observations ($\mathfrak{I}_{\mu-B}$). At lower water uptake (**Figure 6b**), the hydrophilic network is more disconnected at the micrometer scale, leading to increased $\mathfrak{I}_{\mu-B}$. At higher water uptake (**Figure 6c**), the hydrophilic channels expand as in **Figure 6a** to connect more of the dead ends, resulting in larger effective domain size and lower network tortuosity. We are continuing to pursue more detailed NMR, scattering, and microscopy studies in order to understand the origin of the micrometer-scale heterogeneity that leads to the observed diffusion behavior.

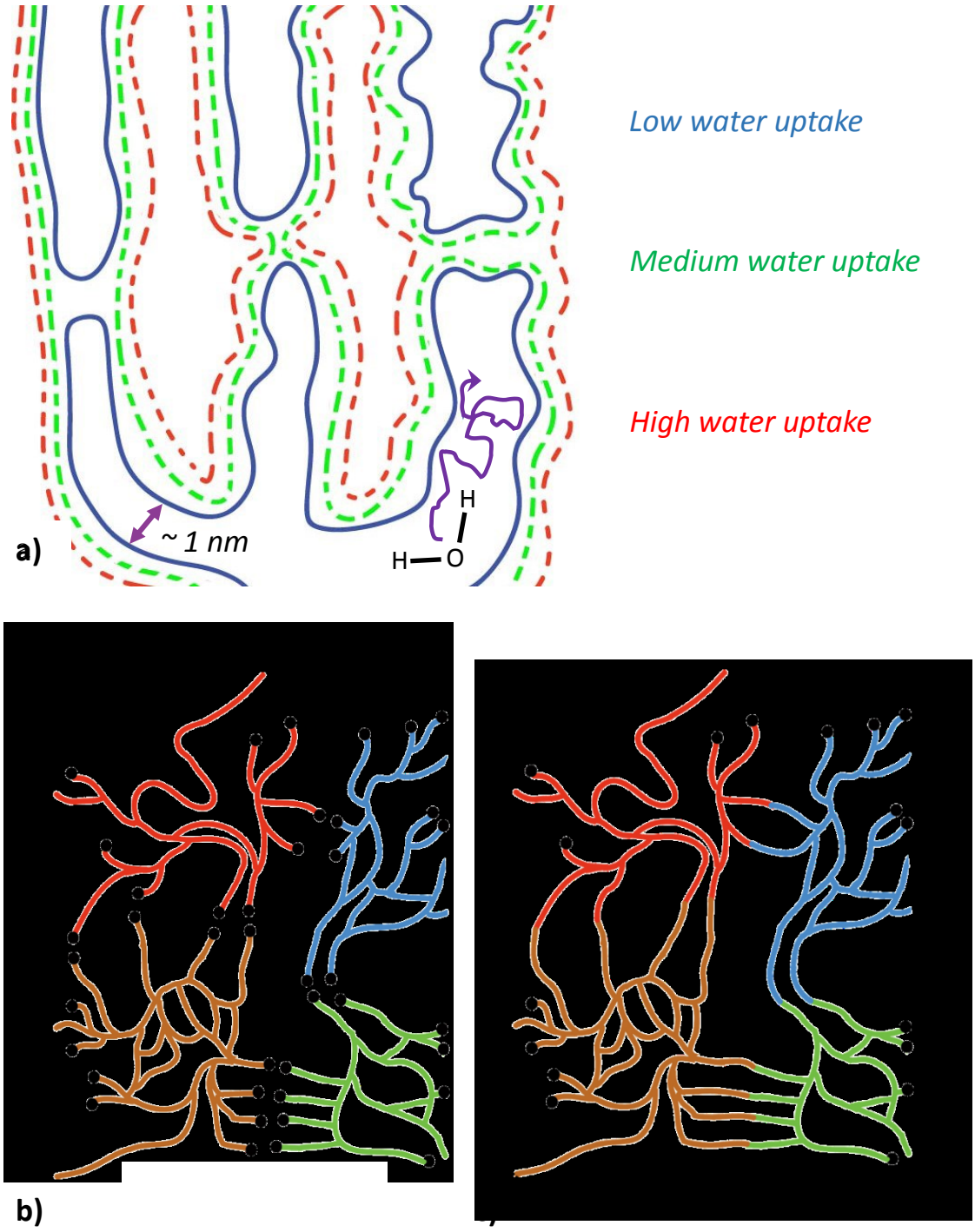


**Figure 6.** Model for multi-scale restricted water transport in AEMs and CEMs. a) Interconnected hydrophilic cavity network on the nanometer scale. The solid blue line represents the hydrophilic network at low hydration, the dashed green and red lines represent the network at increasing levels

of hydration in which cavities become increasingly interconnected. b) Hydrophilic transport network with clusters of dead ends (black dots) that break overall connection pathways and create network boundaries on micrometer scales, as observed by NMR tortuosity measurements. This picture is idealized to show the concept, and this structuring would most likely be more irregular in terms of boundary layer shape. That is, this structuring likely would not have spatial boundaries that consist of simple shapes such as squares, circles, ellipsoids, etc. At sufficiently long diffusion time Δ, water diffusion is restricted by these collections (boundary layers) of dead-ends, leading to a decrease in $D_{H2O}$ (restricted diffusion) and an increase in tortuosity (both $\Im_{\mu-B}$ and $\Im_{L-B}$). c) At high water uptake, hydrophilic cavities expand to connect more dead ends and form more continuous pathways, leading to decreased tortuosity of the network.

***Water content, counterion type, and membrane chemistry effects on diffusion***

**Figure 7** shows the relationship between the water self-diffusion coefficient, $D_{H2O}$, and water volume fraction, $\phi$, for AEMs and CEMs. The filled squares and triangles represent AEM_OH (samples with $OH^-$ counter-ion) and AEM_Br (samples with $Br^-$ counter-ion), respectively, while the red and black unfilled symbols represent CEM_H (samples with $H^+$ counter-ion) and CEM_K (samples with $K^+$ counter-ion). Nafion in the proton form is used as a reference sample. **Figure 7a** compares $D_{H2O}$ for AEM_OH and CEM_H (see also **Figure S2a**). Among the AEM samples, AEM_BTMA_OH exhibits the highest saturated water content, leading to higher $D_{H2O}$, followed by AEM_C6_OH, AEM_C10_OH, and AEM_C16_OH in decreasing order. When alkyl sidechain length increases, water content decreases due to the hydrophobicity of the side chain, which limits water sorption of the AEMs. As shown in **Figure 7a**, all AEM_OHs appear to follow an overlapping trend with $\phi$ (black dashed line to guide the eye). We note here that dependencies of transport on water uptake in terms of $\phi$ should correlate more strongly with

morphological structure since $\phi$ is a bulk-type measurement, while dependencies on uptake in terms of $\lambda$ (water molecules per ionic group, see next section) should reflect local molecular-scale phenomena since $\lambda$ is the local hydration number. Thus, the similar dependence for all samples in terms of the relationship of $D_{H2O}$ with $\phi$ indicates similarity of the connectivity of the hydrophilic network among these membranes. Similarly, all of the CEM_Hs followed a single trend line (red dashed line) and showed faster water diffusion by a factor of ≈ 1.5 relative to the AEM_OHs. We note this factor is similar to the ratio of the proton and hydroxide diffusion coefficient in free aqueous solution,[45] and qualitatively mirrors the $D_{H2O}$ ratio of $CH_3C_6H_4SO_3H$ to $(CH_3)_4NOH$ in free solution (**Figure 4**) where the local water-water and water-ion molecular interactions are the main determining factors for water diffusion.[45-47] However, in a membrane, both the local interactions and the morphology (hydrophilic network heterogeneity) influence $D_{H2O}$. This leads, in general, to the differing ratio of water diffusion coefficients in ionic polymer membranes as compared to aqueous solution. Nafion shows the highest self-diffusion coefficient of water compared to CEM_H and AEM_OH, although it absorbed less water, presumably due to its strongly interconnected nanophase-separated hydrophilic channel structure[18-20] as well as its fast local transport.[40]

**Figure 7b** compares the self-diffusion coefficient of water in CEM_K and CEM_H. Increasing the degree of functionalization of CEMs leads to an increase in the water uptake of the membranes, resulting in faster water self-diffusion. CEM_Hs showed overall slower water self-diffusion than CEM_Ks, likely due to the energetics of hydration and differing ion association of the sulfonate-proton pair as compared to the sulfonate-potassium ion pair. As shown in **Figure 7c**, AEM_OH showed overall slower water diffusion behavior as compared to AEM_Br, and this deviation is most pronounced for the BTMA membranes. Water will have a weaker interaction

with $Br^-$ than $OH^-$ and the cation-anion pairing may be different between $Br^-$ and $OH^-$ and the ammonium cation, leading to different water hydration behaviors. These factors will enable water to diffuse faster in the $Br^-$ form membranes as compared to the $OH^-$ form.

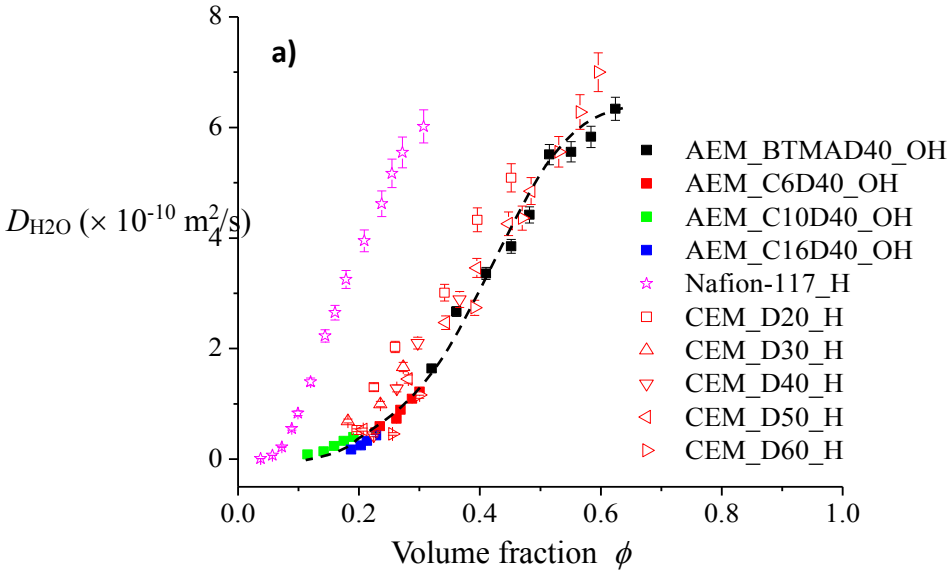


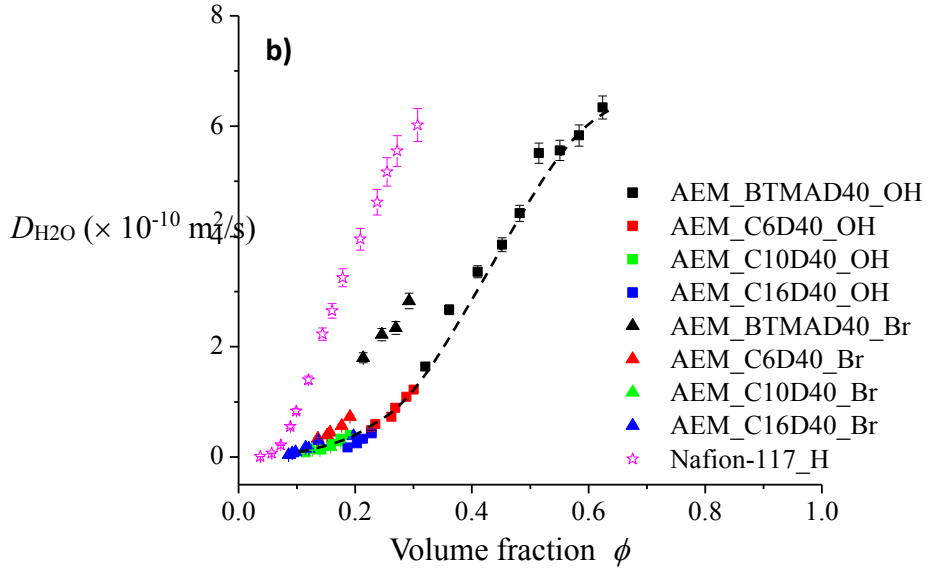

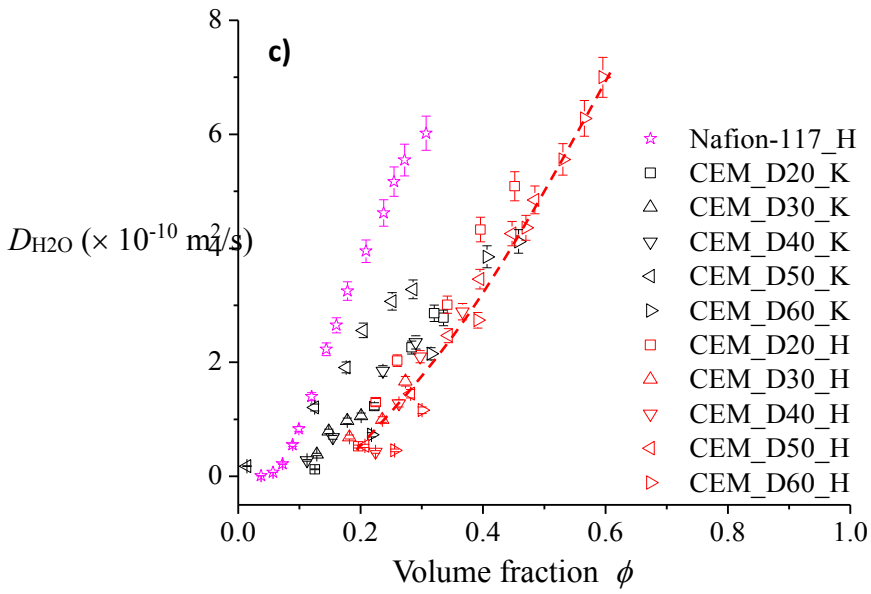


**Figure 7.** Diffusion coefficients of $H_2O$ ($D_{H2O}$) in AEMs and CEMs obtained by $^1H$ NMR diffusometry as a function of volume fraction water $\phi$. a) AEM_OH (samples with $OH^-$ counter-ion) vs. CEM_H (samples with $H^+$ counter-ion). b) CEM_H vs. CEM_K. c) AEM_Br vs. AEM_OH. We used Nafion as a reference sample. AEM_OH and CEM_H membranes appear to follow overlapping trends (master curves), shown by the dashed lines (black and red, guides to the eye), although CEM_H materials show somewhat faster diffusion than AEM_OH. CEM_K and AEM_Br show somewhat faster diffusion behavior than their CEM_H and AEM_OH counterparts, indicating a substantial effect of counterion type on interactions of water with the hydrophilic cavities (transport network). Error bars for diffusion coefficient measurement range from ±5% for high water content and ±10% for low water content. All measurements were performed at 22°C and using an intermediate diffusion time Δ = 100 ms.

***Diffusion coefficient of water vs. λ***

To further understand local water-ion-polymer interactions in these membranes, we plot $D_{H2O}$ as a function of $\lambda$, the water–ion molar ratio of $H_2O$ per quaternary ammonium (cationic) or

sulfonate (anionic) site (**Figure 8**). $\lambda$ also relates to the IEC of the membrane (meq/g), water uptake of the membrane (wt%), and molar mass of water $M_{water}$ (g/mol), as shown above in **Equation 3**.

As presented above (**Figure 4**), we measure $D_{H2O}$ in a set of soluble small-molecule analogs to the internal molecular environment of AEMs and CEMs: (1) trifluoromethanesulfonic acid ($CF_3SO_3H$) as an analog to Nafion, (2) p-toluenesulfonic acid ($CH_3C_6H_4SO_3H$) as an analog to sulfonated polyether sulfone CEM, and (3) tetramethylammonium hydroxide ($(CH_3)_4NOH$) as an analog to quaternary ammonium PPO AEM. Our group and others have previously used $CF_3SO_3H$ as an analog to understand the internal environment of perfluorosulfonate ionomers (PFSIs),[40, 48] We are moving toward quantitative models for the interplay of nanoconfinement and local molecular composition, but for these AEMs and CEMs we focus on molecular effects and leave the discussion of confinement to a future publication. For these analog solutions (**Figure 4**), at high $\lambda$ (> 15), $D_{H2O}$ in $(CH_3)_4NOH$ approaches that of $CH_3C_6H_4SO_3H$, while at low $\lambda$, $D_{H2O}$ in $(CH_3)_4NOH$ falls below that of $CH_3C_6H_4SO_3H$ and is approximately half that of $CH_3C_6H_4SO_3H$ at $\lambda$ = 7.5. $CF_3SO_3H$ solutions exhibit the highest $D_{H2O}$, followed by $CH_3C_6H_4SO_3H$, and $(CH_3)_4NOH$. The remarkable water diffusion in $CF_3SO_3H$ is ascribed to its superacidity ($pK_a \sim -14$),[49] and this local intermolecular effect undoubtedly contributes to superior water transport in Nafion.[40, 48]

**Figure 8a** compares the water diffusion behavior of $OH^-$ form AEMs (AEM_OH) and $H^+$ form CEMs (CEM_H). Similar to the trends in water diffusion for the small molecules $CF_3SO_3H$, $CH_3C_6H_4SO_3H$, and $(CH_3)_4NOH$ in solution, Nafion also shows the fastest diffusion, followed by slower diffusion in CEMs and then the slowest observed diffusion values in AEMs. In contrast to the dependencies of $D_{H2O}$ as a function of $\phi$ (**Figure 7**), water diffusion in AEMs and CEMs as a

function of $\lambda$ do not follow overlapping trends. CEM_D20_H has the lowest ion density (IEC) among all of these membranes, which leads to the lowest $D_{H2O}$ curve in **Figure 8a**, and CEM_D60_H with the highest IEC has the highest overall $D_{H2O}$ curve. **Figure S2b** shows the monotonic increase of $D_{H2O}$ vs. $\lambda$ curves with increasing IEC for CEMs. AEMs show a similar trend of increasing $D_{H2O}$ with IEC, with C16 having the lowest IEC and $D_{H2O}$, and with monotonically increasing curves in order of C6, C10, and BTMA.

**Figure 8b** shows the diffusion of CEM_K and CEM_H vs. $\lambda$. Generally, the CEM_K curves overlap the CEM_H curves because of their similar IECs and local water diffusion environment. Clearly, when the degree of functionalization (ion density or IEC) increases, maximum water absorption also increases leading to faster diffusion.

**Figure 8c** compares the water self-diffusion coefficient vs. $\lambda$ for AEM_Br and AEM_OH (see also **Figure S2b**). Similar to CEMs, the different AEMs do not follow an overlapping trend, as shown in **Figure 7b**. This arises due to the variation of local molecular environments for water transport, most likely modulated by alkyl sidechain length, counterion type, and IEC. Further systematic study will be needed to understand the details of these subtle molecular-scale effects.

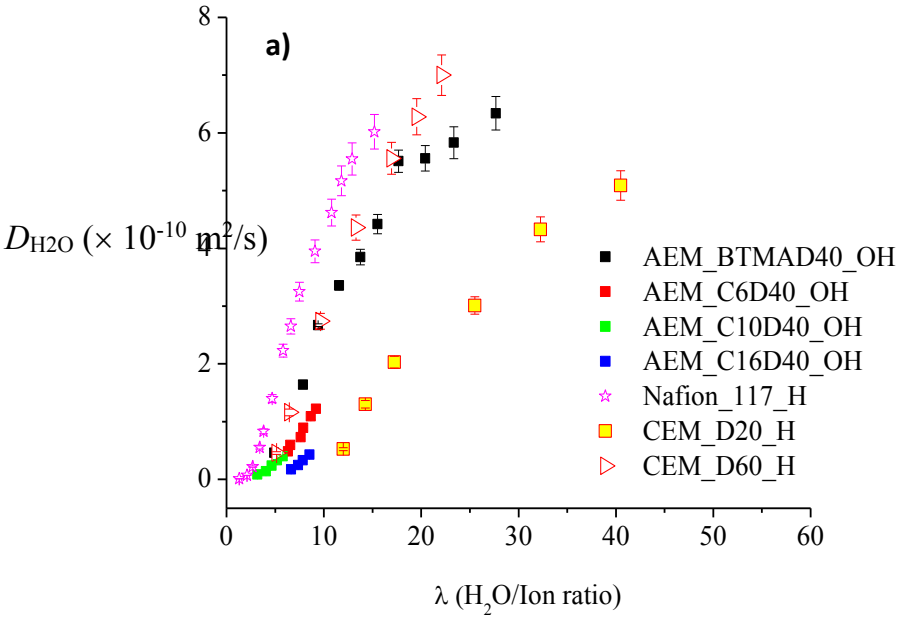
a)
$D_{H2O}$ (× $10^{-10}$ $m^2$/s)
λ ($H_2O$/Ion ratio)
AEM_BTMAD40_OH
AEM_C6D40_OH
AEM_C10D40_OH
AEM_C16D40_OH
Nafion_117_H
CEM_D20_H
CEM_D60_H

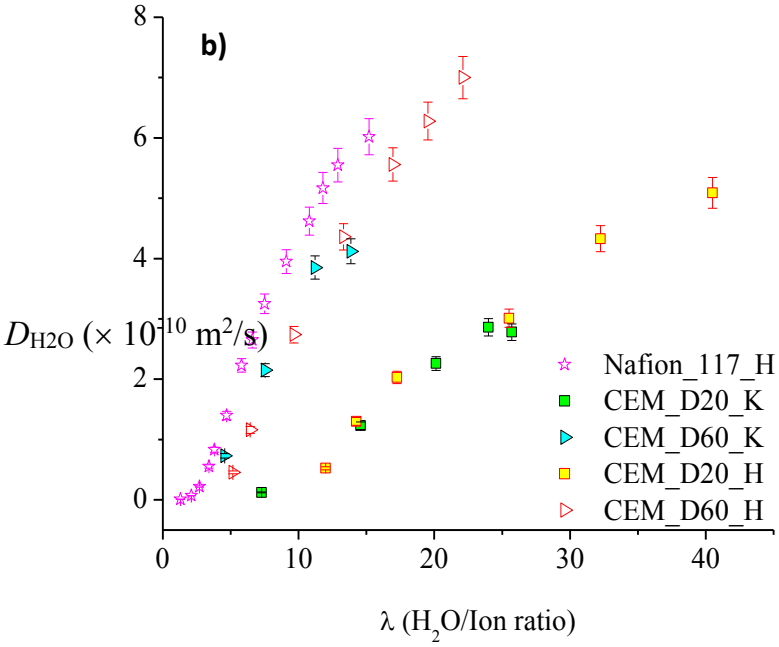
b)
$D_{H2O}$ (× $10^{-10}$ $m^2$/s)
λ ($H_2O$/Ion ratio)
Nafion_117_H
CEM_D20_K
CEM_D60_K
CEM_D20_H
CEM_D60_H

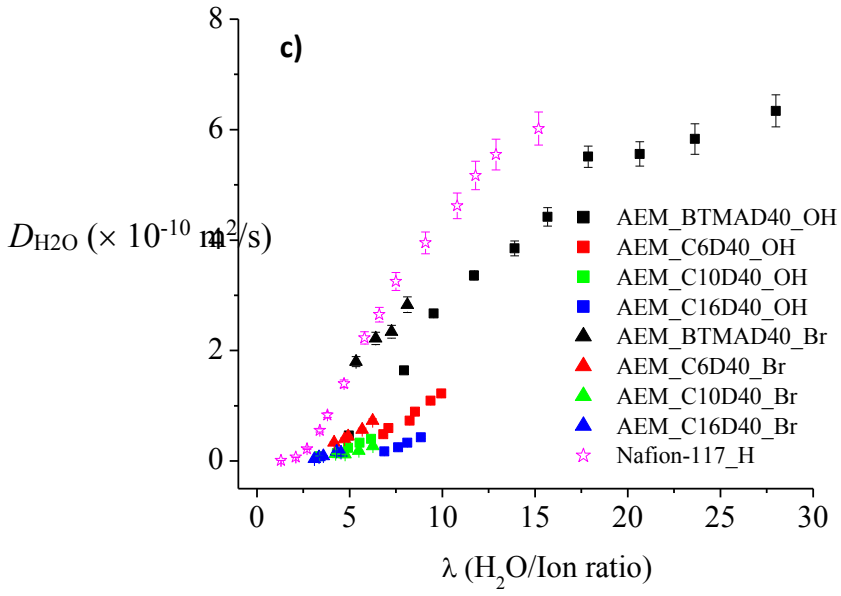


**Figure 8.** $D_{H2O}$ in AEMs and CEMs obtained by $^1$H NMR diffusometry as a function water-ion mole ratio $\lambda$. a) AEM_OH vs. CEM_H. b) CEM_H vs. CEM_K. c) AEM_Br vs. AEM_OH. We used Nafion as a reference sample. AEM_OHs and CEM_Hs do not follow overlapping trend (master) curves as in Figure 7. The relationship between $D_{H2O}$ and $\lambda$ indicates that variations between membranes arise from differences in local ion-water interactions driven mostly by ion density (IEC). Error bars for $D_{H2O}$ measurement are ±5% for high water content and ±10% for low water content. All measurements were performed at 22°C and using $\Delta$ = 100 ms.

In short, the differences of diffusion behavior observed as a function of water $\phi$ and of $\lambda$ can expose general pictures of hydrophilic network heterogeneity (morphology) and local molecular (ion–water) interactions. *Regarding $\phi$ dependencies,* AEM_OH and CEM_H appear to follow the same curve, indicating similarities between their hydrophilic domain morphologies. Varying counter ion type affects transport in both AEMs and CEMs. Water diffusion in CEMs, in general, is faster than AEMs. Water diffusion in CEM_K is faster than CEM_H, and water diffusion in AEM_Br is faster than AEM_OH. *Regarding $\lambda$ dependencies,* molecular interactions

between counterions, polymer-fixed ionic sites, alkyl sidechains, and water drive substantial variations in bulk water transport. For AEMs, counterion type and alkyl sidechain length drive substantial changes in local transport, while in CEMs we vary degree of functionalization, which produces a much stronger variation in local transport than counterion type change.

## Conclusions

We have investigated water transport properties of a range of random copolymer cation-exchange and anion-exchange membranes (CEMs and AEMs) as a function of counterion type, alkyl side chain length, and hydration level. Our detailed NMR diffusometry measurements demonstrate that water self-diffusion coefficients can vary dramatically with composition, and with the length scale of the diffusion measurement.

Based on varying the diffusion time, $\Delta$, (and thus the length scale probed) we observe restricted diffusion in all membrane samples (except in the benchmark Nafion). Furthermore, we introduce two separate tortuosity parameters, one averaged from local, nm-scale to bulk ($\Im_{L-B}$) and one averaged from μm-scale to bulk ($\Im_{\mu-B}$), and these enable us to separately quantify the effects of material heterogeneity on transport over these different length scales. We introduce a qualitative model that is consistent with our tortuosity results and involves two parts: 1) water swelling increases the local (nm-scale) connectivity of the hydrophilic cavities (e.g., bridging dead ends), which in turn decreases the tortuosity and increases bulk transport, and 2) heterogeneous clusters of pathway dead ends, which form effective boundaries to diffusion, are distributed such that there is a strong tortuosity effect observed on micrometer scales.

By plotting water diffusion coefficient as a function of water volume fraction, $\phi$, we gain more insight into how transport is influenced by water-swollen domain structuring. In a complementary way, by plotting water self-diffusion coefficient as a function of the water-ion

molar ratio $\lambda$, we gain insight into how local intermolecular interactions affect transport. The different AEMs, in particular, show an overlapping trend of water diffusion vs. volume fraction $\phi$ (but not vs. $\lambda$), indicating a common heterogeneity of their hydrophilic network across these membranes. Water diffusion in CEMs is generally faster than in AEMs, which arises from faster local molecular transport effects in CEMs, even though from our studies AEMs exhibit more favorable network connectivity (heterogeneity) on scales larger than a few nm.

This sort of nm-scale to μm-scale information – the connection of average structural features and bulk transport in heterogeneous materials – is not readily available by scattering or microscopy techniques, although those techniques can complement diffusometry studies to connect structural and transport information. We note that a focused study using micrometer-scale SANS (microSANS) or ultra-small angle X-ray scattering (USAXS) might provide insight into these heterogeneities. Extensions of this study by NMR are already underway to gain more deep mechanistic information regarding the origins of the tortuosity and structural heterogeneities in these materials. As part of such extensions, we are beginning to explore the self-assembly process of the nm-scale hydrophilic networks and other molecular-structure-driven differences between fixed-anion and fixed-cation systems in order to gain fundamental insight into the causes for differences in multi-scale transport behaviors between CEM and AEM membranes. Understanding the multi-scale phenomena that contribute to bulk water and ion transport in polymer membranes will help drive us toward the production of inexpensive and highly efficient membranes for fuel cells and a range of molecular and ionic separations.

## Supporting Information

Example 1D NMR spectral slices from a diffusometry experiment; Diffusion coefficients for water in membranes as a function of water volume fraction, weight percent, and water-ion mole

ratio; Tabulated densities and tortuosities for AEMs and CEMs; Tabulated diffusion coefficients for solutions of tetramethylammonium hydroxide, p-toluenesulfonic acid, and trifluoromethanesulfonic acid; Additional restricted diffusion data and Mitra analysis; SAXS of selected dry AEMs and CEMs.

## Acknowledgements

This work was supported by the National Science Foundation under award numbers DMR 1507764 and 1810194. Additional support was provided by the Advanced Research Projects Agency – Energy (ARPA-E), U.S. Department of Energy, under award number: DE-AR0000121 and the U.S. National Science Foundation DMREF program under award number CHE-1534326. Any opinions, findings and conclusions or recommendations expressed in this material are those of the author(s) and do not necessarily reflect the views of the National Science Foundation (NSF). We also thank Professor Paul A. Deck for assistance with anerobic ($OH^-$ exchange) membrane sample preparation and helpful discussions.

## References

1. Schäfer, A.; Heywood, J. B.; Weiss, M. A., Future fuel cell and internal combustion engine automobile technologies: A 25-year life cycle and fleet impact assessment. *Energy* **2006,** *31* (12), 2064-2087.
2. Scherer, G. n. G., *Fuel cells I*. Springer: New York ; London, 2008
3. Maurya, S.; Shin, S. H.; Kim, Y.; Moon, S. H., A review on recent developments of anion exchange membranes for fuel cells and redox flow batteries. *Rsc Advances* **2015,** *5* (47), 37206-37230.
4. Mauritz, K. A.; Moore, R. B., State of understanding of Nafion. *Chemical Reviews* **2004,** *104* (10), 4535-4585.
5. Bashyam, R.; Zelenay, P., A class of non-precious metal composite catalysts for fuel cells. *Nature* **2006,** *443* (7107), 63-66.
6. Wu, G.; Johnston, C. M.; Mack, N. H.; Artyushkova, K.; Ferrandon, M.; Nelson, M.; Lezama-Pacheco, J. S.; Conradson, S. D.; More, K. L.; Myers, D. J.; Zelenay, P., Synthesis-structure-performance correlation for polyaniline-Me-C non-precious metal cathode catalysts for oxygen reduction in fuel cells. *Journal of Materials Chemistry* **2011,** *21* (30), 11392-11405.

7. Li, X. M.; Hao, X. G.; Abudula, A.; Guan, G. Q., Nanostructured catalysts for electrochemical water splitting: current state and prospects. *Journal of Materials Chemistry A* **2016,** *4* (31), 11973-12000.
8. Shao, M. H.; Chang, Q. W.; Dodelet, J. P.; Chenitz, R., Recent Advances in Electrocatalysts for Oxygen Reduction Reaction. *Chemical Reviews* **2016,** *116* (6), 3594-3657.
9. Miller, H. A.; Lavacchi, A.; Vizza, F.; Marelli, M.; Di Benedetto, F.; Acapito, F. D. I.; Paska, Y.; Page, M.; Dekel, D. R., A Pd/C-CeO2 Anode Catalyst for High-Performance Platinum-Free Anion Exchange Membrane Fuel Cells. *Angewandte Chemie-International Edition* **2016,** *55* (20), 6004-6007.
10. Lu, S. F.; Pan, J.; Huang, A. B.; Zhuang, L.; Lu, J. T., Alkaline polymer electrolyte fuel cells completely free from noble metal catalysts. *Proceedings of the National Academy of Sciences of the United States of America* **2008,** *105* (52), 20611-20614.
11. Varcoe, J. R.; Slade, R. C. T.; Wright, G. L.; Chen, Y. L., Steady-state dc and impedance investigations of H-2/O-2 alkaline membrane fuel cells with commercial Pt/C, Ag/C, and Au/C cathodes. *J. Phys. Chem. B* **2006,** *110* (42), 21041-21049.
12. Hickner, M. A.; Herring, A. M.; Coughlin, E. B., Anion Exchange Membranes: Current Status and Moving Forward. *Journal of Polymer Science Part B-Polymer Physics* **2013,** *51* (24), 1727-1735.
13. Zhu, L.; Pan, J.; Wang, Y.; Han, J. J.; Zhuang, L.; Hickner, M. A., Multication Side Chain Anion Exchange Membranes. *Macromolecules* **2016,** *49* (3), 815-824.
14. Pan, J.; Zhu, L.; Han, J.; Hickner, M. A., Mechanically Tough and Chemically Stable Anion Exchange Membranes from Rigid-Flexible Semi-Interpenetrating Networks. *Chemistry of Materials* **2015,** *27* (19), 6689-6698.
15. Zhu, L.; Zimudzi, T. J.; Li, N. W.; Pan, J.; Lin, B. C.; Hickner, M. A., Crosslinking of comb-shaped polymer anion exchange membranes via thiol-ene click chemistry. *Polymer Chemistry* **2016,** *7* (14), 2464-2475.
16. Mohanty, A. D.; Lee, Y.-B.; Zhu, L.; Hickner, M. A.; Bae, C., Anion Exchange Fuel Cell Membranes Prepared from C–H Borylation and Suzuki Coupling Reactions. *Macromolecules* **2014,** *47* (6), 1973-1980.
17. Jiao, K.; Li, X. G., Water transport in polymer electrolyte membrane fuel cells. *Prog. Energy Combust. Sci.* **2011,** *37* (3), 221-291.
18. Li, J.; Park, J. K.; Moore, R. B.; Madsen, L. A., Linear coupling of alignment with transport in a polymer electrolyte membrane. *Nature Materials* **2011,** *10* (7), 507-511.
19. Hou, J. B.; Li, J.; Mountz, D.; Hull, M.; Madsen, L. A., Correlating morphology, proton conductivity, and water transport in polyelectrolyte-fluoropolymer blend membranes. *Journal of Membrane Science* **2013,** *448*, 292-299.
20. Li, J.; Wilmsmeyer, K. G.; Madsen, L. A., Anisotropic Diffusion and Morphology in Perfluorosulfonate Ionomers Investigated by NMR. *Macromolecules* **2009,** *42* (1), 255-262.
21. Hou, J.; Li, J.; Madsen, L. A., Anisotropy and Transport in Poly(arylene ether sulfone) Hydrophilic−Hydrophobic Block Copolymers. *Macromolecules* **2010,** *43* (1), 347-353.
22. Marino, M. G.; Melchior, J. P.; Wohlfarth, A.; Kreuer, K. D., Hydroxide, halide and water transport in a model anion exchange membrane. *Journal of Membrane Science* **2014,** *464*, 61-71.
23. Hibbs, M. R.; Hickner, M. A.; Alam, T. M.; McIntyre, S. K.; Fujimoto, C. H.; Cornelius, C. J., Transport Properties of Hydroxide and Proton Conducting Membranes. *Chemistry of Materials* **2008,** *20* (7), 2566-2573.

24. Janarthanan, R.; Horan, J. L.; Caire, B. R.; Ziegler, Z. C.; Yang, Y.; Zuo, X. B.; Liberatore, M. W.; Hibbs, M. R.; Herring, A. M., Understanding Anion Transport in an Aminated Trimethyl Polyphenylene with High Anionic Conductivity. *Journal of Polymer Science Part B-Polymer Physics* **2013,** *51* (24), 1743-1750.
25. Li, N.; Leng, Y.; Hickner, M. A.; Wang, C.-Y., Highly Stable, Anion Conductive, Comb-Shaped Copolymers for Alkaline Fuel Cells. *Journal of the American Chemical Society* **2013,** *135* (27), 10124-10133.
26. Wang, F.; Hickner, M.; Kim, Y. S.; Zawodzinski, T. A.; McGrath, J. E., Direct polymerization of sulfonated poly(arylene ether sulfone) random (statistical) copolymers: candidates for new proton exchange membranes. *Journal of Membrane Science* **2002,** *197* (1), 231-242.
27. Stejskal, E. O.; Tanner, J. E., Spin Diffusion Measurements: Spin Echoes in the Presence of a Time-Dependent Field Gradient. *Journal of Chemical Physics* **1965,** *42* (1), 288-+.
28. Einstein, A., Über die von der molekularkinetischen Theorie der Wärme geforderte Bewegung von in ruhenden Flüssigkeiten suspendierten Teilchen. *Annalen der Physik* **1905,** *322* (8), 549-560.
29. Callaghan, P. T., *Translational dynamics and magnetic resonance : principles of pulsed gradient spin echo NMR*. Oxford University Press: Oxford ; New York, 2011
30. Zhang, J. H.; Giotto, M. V.; Wen, W. Y.; Jones, A. A., An NMR study of the state of ions and diffusion in perfluorosulfonate ionomer. *Journal of Membrane Science* **2006,** *269* (1-2), 118-125.
31. Hou, J.; Madsen, L. A., New insights for accurate chemically specific measurements of slow diffusing molecules. *The Journal of Chemical Physics* **2013,** *138* (5), 054201.
32. Price, W. S., Pulsed-field gradient nuclear magnetic resonance as a tool for studying translational diffusion: Part 1. Basic theory. *Concepts in Magnetic Resonance* **1997,** *9* (5), 299-336.
33. Valiullin, R., *Diffusion NMR of confined systems : fluid transport in porous solids and heterogeneous materials*. Royal Society of Chemistry: Cambridge, 2017
34. Mitra, P. P.; Sen, P. N.; Schwartz, L. M., Short-time behavior of the diffusion coefficient as a geometrical probe of porous media. *Physical Review B* **1993,** *47* (14), 8565-8574.
35. Barrie, P. J., Characterization of porous media using NMR methods. In *Annual Reports on Nmr Spectroscopy, Vol 41*, Webb, G. A., Ed. Elsevier Academic Press Inc: San Diego, 2000; Vol. 41, pp 265-316.
36. Lin, G. X.; Aucoin, D.; Giotto, M.; Canfield, A.; Wen, W. Y.; Jones, A. A., Lattice model simulation of penetrant diffusion along hexagonally packed rods in a barrier matrix as determined by pulse-field-gradient nuclear magnetic resonance. *Macromolecules* **2007,** *40* (5), 1521-1528.
37. Timachova, K.; Villaluenga, I.; Cirrincione, L.; Gobet, M.; Bhattacharya, R.; Jiang, X.; Newman, J.; Madsen, L. A.; Greenbaum, S. G.; Balsara, N. P., Anisotropic Ion Diffusion and Electrochemically Driven Transport in Nanostructured Block Copolymer Electrolytes. *The Journal of Physical Chemistry B* **2018,** *122* (4), 1537-1544.
38. Park, M. J.; Balsara, N. P., Anisotropic Proton Conduction in Aligned Block Copolymer Electrolyte Membranes at Equilibrium with Humid Air. *Macromolecules* **2010,** *43* (1), 292-298.
39. Shen, L.; Chen, Z. X., Critical review of the impact of tortuosity on diffusion. *Chemical Engineering Science* **2007,** *62* (14), 3748-3755.

40. Lingwood, M. D.; Zhang, Z. Y.; Kidd, B. E.; McCreary, K. B.; Hou, J. B.; Madsen, L. A., Unraveling the local energetics of transport in a polymer ion conductor. *Chemical Communications* **2013,** *49* (39), 4283-4285.
41. Ohkubo, T.; Kidena, K.; Ohira, A., Determination of a Micron-Scale Restricted Structure in a Perfluorinated Membrane from Time-Dependent Self-Diffusion Measurements. *Macromolecules* **2008,** *41* (22), 8688-8693.
42. Yu, Z.; He, Y.; Wang, Y.; Madsen, L. A.; Qiao, R., Molecular Structure and Dynamics of Ionic Liquids in a Rigid-Rod Polyanion-Based Ion Gel. *Langmuir* **2017,** *33* (1), 322-331.
43. Wang, Y.; Chen, Y.; Gao, J. W.; Yoon, H. G.; Jin, L. Y.; Forsyth, M.; Dingemans, T. J.; Madsen, L. A., Highly Conductive and Thermally Stable Ion Gels with Tunable Anisotropy and Modulus. *Advanced Materials* **2016,** *28* (13), 2571-2578.
44. Kidd, B. E.; Forbey, S. J.; Steuber, F. W.; Moore, R. B.; Madsen, L. A., Multiscale Lithium and Counterion Transport in an Electrospun Polymer-Gel Electrolyte. *Macromolecules* **2015,** *48* (13), 4481-4490.
45. Tuckerman, M.; Laasonen, K.; Sprik, M.; Parrinello, M., Ab initio molecular dynamics simulation of the solvation and transport of hydronium and hydroxyl ions in water. *The Journal of Chemical Physics* **1995,** *103* (1), 150-161.
46. Zundel, G.; Metzger, H., Energy Bands of Excess Tunneling Protons in Fluid Acids: IR Spectroscopy of H5O2+ Groups. *Zeitschrift Fur Physikalische Chemie-Frankfurt* **1968,** *58* (5-6), 225-&.
47. Eigen, M., Proton Transfer Acid-Base Catalysis + Enzymatic Hydrolysis I: Elementary Processes. *Angewandte Chemie-International Edition* **1964,** *3* (1), 1-&.
48. Paddison, S. J.; Paul, R.; Zawodzinski, T. A., Proton friction and diffusion coefficients in hydrated polymer electrolyte membranes: Computations with a non-equilibrium statistical mechanical model. *Journal of Chemical Physics* **2001,** *115* (16), 7753-7761.
49. Company, C. R., CRC handbook of chemistry and physics. 94th ed.; CRC Press.: Boca Raton, Fla. etc.

# Multiscale Tortuous Diffusion in Anion and Cation Exchange Membranes

*Lam M. Thieu,*[a] *Liang Zhu,*[b] *Andrew G. Korovich,*[a]

*Michael A. Hickner,*[b] *and Louis A. Madsen,**[a]

[a]Department of Chemistry and Macromolecules Innovation Institute, Virginia Tech, Blacksburg, VA, 24060

[b]Department of Materials Science and Engineering, The Pennsylvania State University, University Park, PA, 16802

**For Table of Contents use only:**